Room-temperature ferromagnetism of sol-gel-synthesized $Sn_{1-x}{}^{57}Fe_xO_{2-\delta}$ powders

K. Nomura,[1] C. A. Barrero,[1,2,*] J. Sakuma,[3] and M. Takeda[3]
[1]*School of Engineering, The University of Tokyo, 7-3-1 Hongo, Bunkyo-ku, Tokyo 113-8656, Japan*
[2]*Grupo de Estado Sólido, Sede de Investigación Universitaria, Universidad de Antioquia, A.A. 1226, Medellín, Colombia*
[3]*Faculty of Science, Toho University, 2-2-1 Miyama, Funabashi-city, Chiba, 274-0072, Japan*
(Received 14 August 2006; revised manuscript received 23 January 2007; published 11 May 2007)

We report unusual observations in the magnetic behavior of $Sn_{1-x}{}^{57}Fe_xO_{2-\delta}$ powders prepared by a sol-gel method. Mössbauer spectra showed three different sites for those irons in the SnO_2 lattice. The samples seem to exhibit many sources of ferromagnetism, and the dominance of one of them greatly depends upon the synthesis conditions. In one sample, prepared using citric acid solution of metal Fe and annealed at 500 °C for two hours, we observed magnetization, but its room temperature Mössbauer spectrum did not show any magnetic component, suggesting that the ferromagnetism could not have originated from the iron ions but from magnetic defects. In another sample prepared from chloride acid solution of Fe_2O_3 and annealed at 600 °C for six hours, a large magnetization and a sextet with broad lines were observed and the ferromagnetism was ascribed to iron impurities. In another sample prepared from citric acid solution of metal Fe but annealed at 650 °C for two hours, we observed an intensive magnetic sextet with sharp lines but small magnetization, suggesting the presence of hematite doped with tin.

DOI: 10.1103/PhysRevB.75.184411 PACS number(s): 75.25.+z, 75.50.Pp, 73.63.Bd

I. INTRODUCTION

Understanding the origin of the magnetic interactions in diluted magnetic semiconductors (DMS) is actually a subject of intensive research and it is greatly enhancing our basic knowledge of magnetism.[1–5] Many theories have been put forward and this subject is still a matter of controversy. Most of the reported models are based upon the interactions between magnetic impurities, which can be mediated either by oxygens, or by free carriers. Defects in DMS can also contribute to the measured saturation magnetization. There have been reports in un-doped semiconductors for which defects can be the unique source of ferromagnetism,[6] or they can induce magnetic moments in the cations of the host lattice, which are nonmagnetic.[7] Moreover, there have been cases for which the doping of semiconductors with nonmagnetic ions can induce ferromagnetism.[8,9] Here, we report on one case in which the magnetic impurities in a DMS material are not the main source of ferromagnetism, but the defects. Moreover, our samples seem to exhibit different sources of magnetism, originating from impurity ferric ions, defects or impurity compounds. The main source of ferromagnetism in a given sample seems to be dictated by the synthesis conditions.

Now, after the report of room temperature ferromagnetism in Co-doped TiO_2 films,[10] intensive experimental and theoretical research started on rutile type oxide DMS.[11,12] Kimura *et al.*[13] investigated thin films Mn doped SnO_2 but no ferromagnetism was observed. Ogale *et al.*[14] reported that pulsed laser deposited thin film of 5 at. % Co doped SnO_2 shows high temperature ferromagnetism with a giant cobalt moment. On the other hand, deposited thin films of SnO_2 doped with Fe showed remarkable strong ferromagnetism, for which a novel ferromagnetic exchange mechanism is considered.[15] Fitzgerald *et al.*[16] have measured room temperature ferromagnetism in bulk ceramic Mn-, Co-, and Fe-doped SnO_2. In spite of the fact that some minor amounts of impurity compounds were detected, the magnetization could not be attributed to their presence, but to the transition metals substituting tin in SnO_2. Chemically synthesized powders of SnO_2 doped with Co and Fe have been studied by Punnoose *et al.*[17,18] and Hays *et al.*[19] The authors suggest a close relationship between the structural and magnetic properties in Fe-doped SnO_2 nanoparticles. In all of these works, the observed ferromagnetism has been attributed to interactions between the magnetic impurities, but never has the main source been associated to magnetically ordered defects. In the case of Fe doped SnO_2, the Mössbauer spectra for those samples exhibiting magnetization always consist of a sextet, besides a strong doublet. This sextet component is attributed to the magnetically ordered iron ions, which are the main source of ferromagnetism. Here we report the case of one sample for which magnetization is clearly observed but the Mössbauer spectrum does not exhibit any sextet component, thus suggesting that defects can be perhaps the main source of ferromagnetism even in the presence of the magnetic iron ions.

Most DMS materials have been prepared as thin films, but if ferromagnetism is an intrinsic property, then it should be possible to measure the same properties in the material prepared in powdered form. Thus another purpose of the present investigation is to search for appropriate experimental conditions for obtaining room temperature ferromagnetism in ^{57}Fe doped SnO_2 powders prepared from a sol-gel method. Additionally, Mössbauer spectroscopy is used to reveal the local environment around the iron ions in the SnO_2 lattice, in order to clarify the mechanism for magnetic ordering.

II. EXPERIMENT

Samples of $Sn_{1-x}{}^{57}Fe_xO_{2-\delta}$ with molar ratios of $x=[Fe]/([Sn]+[Fe])=0.0025$, 0.005, 0.01, 0.03, 0.05, 0.1, and 0.15, were obtained by a sol-gel method. The tin solutions were prepared by mixing 20 mL of ethylene glycol, 0.04*M* citric acid, 0.01*M* $Sn(IV)Cl_2(acetylacetate)_2$, and 5 mL of

concentrated HNO_3. The pH was adjusted to 8 by adding NH_4OH (25%). On the other hand, two types of iron solutions were used: either citric acid solutions of dissolved metal ^{57}Fe or chloride acid solutions of dissolved $^{57}Fe_2O_3$. The tin and iron solutions were mixed, evaporated at 80 °C, calcinated at around 200 °C, and finally annealed at different temperatures for different annealing times. The annealing time depended on the color change from black (for the bulk polymeric complex) to pale gray (for the final Fe doped SnO_2 powder). To accomplish this color change, we needed just two hours for the samples coming from the citric acid solutions of metal ^{57}Fe, independent upon the annealing temperature. However, six hours of annealing was required for the samples containing $^{57}Fe_2O_3$. All thermal treatments were performed in air. The products were characterized by XRD, SEM, EDAX, VSM, and Mössbauer spectrometry at different temperatures. XRD patterns were obtained using a MacScience diffractometer equipped with Cu ($K\alpha$) radiation; data were collected in the 15°–70° 2θ range with a 0.02° step and a counting velocity of 2° per minute. The patterns were analyzed using a program called MAUD[20] which combines the Rietveld method and a Fourier transform analysis, well adapted especially in presence of broadened Bragg peaks: this program allows us to derive crystalline cell parameters, average crystallite size and phase abundance. The SnO_2 structural model used was that reported by Baur and Khan.[21] The scale factor, incident intensity, sample displacement, unit cells, three-order polynomial background, the average crystallite size, and phase abundance were refined. The average crystallite size and the texture were assumed to be isotropic and arbitrary, respectively, in the present study. The iterations were performed until convergence was reached. The scanning electron microscopy (SEM) and EDAX studies were performed on HITACHI S-2400 microscope. For EDAX the scan time, accelerating voltage, probe current, electron beam incidence angle, and x-ray take off angle were 180 s, 20 kV, 0.2 nA, 90°, and 31°, respectively. The Mössbauer spectra were collected in a time-mode spectrometer working in the transmission geometry using a constant acceleration drive with triangular reference signal. Calibrations were achieved from a standard α-iron foil at 300 K. The spectra were analyzed using a program called MossWin 3.0. Mössbauer spectra were decomposed into two doublets, magnetic relaxed and sharp sextet components.

III. RESULTS

A. Samples prepared from citric acid solutions of metal ^{57}Fe and annealed at 500 °C and 650 °C for 2 h

The color changes from pale gray to light yellow-orange with the increase of iron content for the samples annealed at 500 °C, and from pale gray to dark orange for samples annealed at 650 °C. The color of the samples is thus affected by both iron content and annealing temperature.

The iron concentrations of the $Sn_{1-x}{}^{57}Fe_xO_{2-\delta}$ samples were determined from EDAX. Three different points in the samples were chosen randomly and about the same iron concentration was obtained for all of them, suggesting homogeneous iron distribution. In fact the sol-gel chemical method has been reported to provide a uniform distribution of the dopant in the host system at low temperatures.[18,22] The EDAX data obtained for some selected samples are listed in Table I. It is seen that the measured concentrations are in reasonable agreement with their nominal compositions.

At low iron doping larger particles with irregular shapes are formed, but as iron content increases the particles start to exhibit fine grains sandy type morphology. Moreover, for low iron content with increasing annealing temperature from 500 °C to 650 °C, the particle sizes seem to increase a little, but at the higher iron concentrations the particle size seems to be same. Average particle sizes of SnO_2 powders as a function of nominal Fe content, estimated from observations of scanning micrographs, are shown in Fig. 1. It is possible to see that particle size decreases with increasing Fe doping. Our results are in good agreement with those reported by Davis *et al.*[22] and by Punnoose *et al.*,[18] who also found decrease of particle size with increasing iron content. Xu *et al.*[23] have also found that most cations, in nanocrystalline SnO_2 restrict grain growth, while a few others, specially Co, have the opposite effect, assisting growth. The increment of iron content in the samples increases the formation of oxygen vacancies as required by charge balancing. This effect, in conjunction also with the lower ionic radii of Fe^{3+} (0.069 nm) in comparison to Sn^{4+} (0.083 nm), can disturb low range crystallographic ordering. On the other hand, as will be shown below, the formation of hematite at the grain surface for the most doped samples and annealed at higher temperatures, could also inhibit additional crystal growing. Another interesting observation is that the effect of the annealing temperature on the particle size is more pronounced at low iron concentrations, i.e., for small iron contents the higher the annealing temperature, the larger the particles sizes. However, as iron increases this effect is lost, and almost all samples exhibit the same particle size independent upon the annealing temperature.

Figure 2 shows the XRD patterns for those samples prepared at 500 °C. The patterns for samples annealed at 650 °C showed similar features. All patterns were adequately fitted by introducing the cassiterite phase of SnO_2, whereas neither SnO nor the metastable orthorhombic phase of SnO_2 was observed. For those samples annealed at 650 °C and having the higher iron contents, an additional hematite phase was introduced. Its presence is clearly demonstrated in Fig. 3, which is the XRD pattern of sample $x=0.15$. If the pattern is plotted in linear scale, the hematite peaks are not clearly noticed, but when plotted in log scale for some expanded regions (see the insets in Fig. 3), they become evident. The structural model used for fitting the hematite phase was that reported by Finger and Hazen.[24] It is worth mentioning that Kundaliya *et al.*[25] have plotted the XRD patterns on log scale to demonstrate the presence of manganese oxides in Mn doped ZnO, whereas Punnoose *et al.*[18] used the same procedure to demonstrate the absence of iron oxides and other impurity phases in the Fe doped SnO_2.

Next, from Fig. 2, it is possible to see that as iron content increases to more than 3% the Bragg peaks increase in broadening, become less intense and shift to lower angles. These effects are more pronounced for those samples prepared at lower annealing temperatures than at higher. These

TABLE I. Summary of the synthesis parameters, EDAX data, and average particle sizes from SEM and XRD.

Nominal Fe (%)	Initial Fe solution	Annealing temperature (°C)	Annealing time (h)	EDAX		Particle size (nm)	
				Fe (%)	Sn (%)	SEM	XRD
0.25	metal Fe	500	2				52
0.5	metal Fe	500	2			225	45
1	metal Fe	500	2			167	52
3	metal Fe	500	2			114	36
5	metal Fe	500	2	5.7	94.3	90	23
10	metal Fe	500	2	10.8	89.2		9
15	metal Fe	500	2	15.8	84.5		12
0.25	metal Fe	650	2				55
0.5	metal Fe	650	2			289	46
1	metal Fe	650	2			258	69
3	metal Fe	650	2			94	95
5	metal Fe	650	2	5.6	94.4	93	97
10	metal Fe	650	2	12.4	87.6		44
15	metal Fe	650	2	18.6	81.4		50
1	Fe_2O_3	600	6			160	25
2	Fe_2O_3	600	6			95	61
6	Fe_2O_3	600	6			96	81
10	Fe_2O_3	600	6	9.1	90.9	63	42

observations suggest that iron ions are incorporated into the SnO_2 lattice, and that crystallinity is improved with increasing temperature. Average crystallite sizes were always smaller than the particle sizes obtained by SEM, thus suggesting polycrystallinity for all samples (see Table I).

Figure 4 shows the variation of the *a* and *c* unit cell parameters as function of the iron nominal content. In general, for all samples, the *c* lattice parameter is always observed to decrease with increasing iron content independent upon the

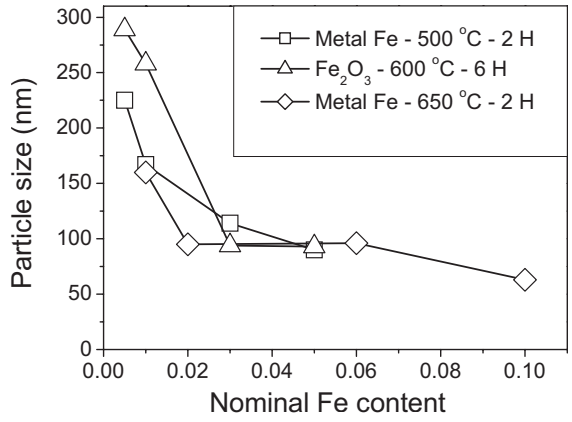

FIG. 1. Average grain sizes from SEM versus iron content for all samples. Square symbols are data for samples coming from citric acid solutions of metal ^{57}Fe and annealed at 500 °C for 2 h. Up triangle symbols are data for samples prepared from HCl solutions of $^{57}Fe_2O_3$ and annealed at 600 °C for 6 h. Diamonds represent for samples prepared using citric acid solutions of metal ^{57}Fe and annealed at 650 °C for 2 h.

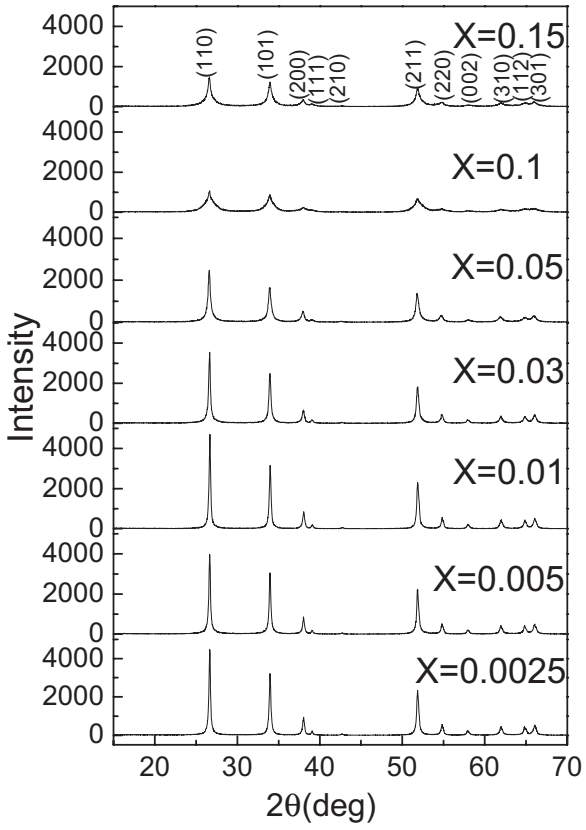

FIG. 2. XRD patterns of $Sn_{1-x}Fe_xO_{2-\delta}$ samples prepared from citric acid solutions of metal ^{57}Fe and annealed at 500 °C for 2 h.

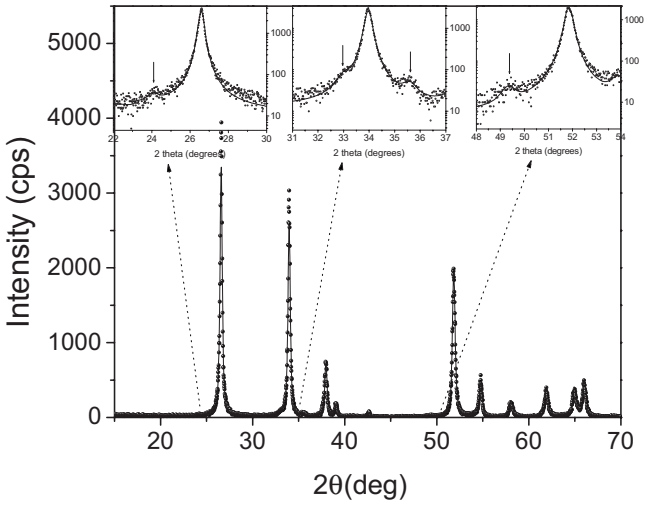

FIG. 3. XRD pattern plotted in linear scale of sample $x=0.15$ prepared using citric acid solution of metal ^{57}Fe and annealed at 650 °C for 2 h. Solid spheres represent the experimental data, whereas the solid lines represent the fit using Rietveld method. The insets show some selected expanded regions plotted in log scale. The arrows point to hematite peaks.

annealing temperature. However, the *a* unit cell changes differently for each series. For those samples annealed at 500 °C, with the exception of samples $x=0.05$ and 0.1, the *a* unit cell remains reasonably constant, but for samples annealed at 650 °C, it decreases up to $x=0.05$ and then increases. This change of the lattice parameters suggests that some iron ions start to be segregated on the surface of SnO_2.

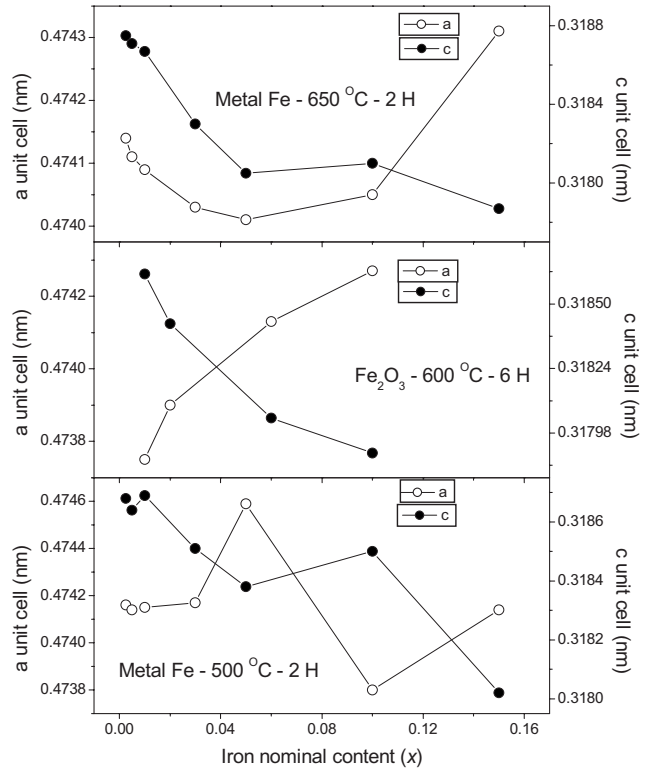

FIG. 4. Changes in the unit cell parameters with increasing iron nominal content for samples prepared from citric acid solutions of metal ^{57}Fe and annealed at 650 °C for 2 h (upper part), HCl solutions of $^{57}Fe_2O_3$ and annealed at 600 °C for 6 h (middle part), and citric acid solutions of metal ^{57}Fe and annealed at 500 °C for 2 h (lower part).

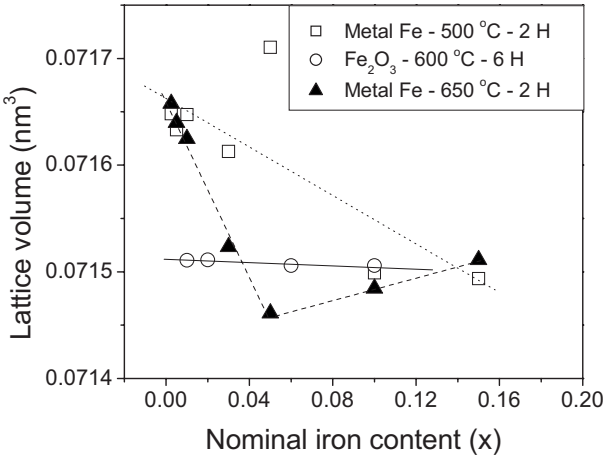

FIG. 5. Lattice volumes versus iron content at different annealing temperatures. Dotted, solid, and dashed lines are linear fits to the data for each group of samples. Open squares represent data for samples coming from citric acid solutions of metal ^{57}Fe and annealed at 500 °C for 2 h. Open circles are data for samples prepared from HCl solutions of $^{57}Fe_2O_3$ and annealed at 600 °C for 6 h. Filled up triangles are for samples prepared using citric acid solutions of metal ^{57}Fe and annealed at 650 °C for 2 h.

Figure 5 shows the variation of the unit cell volume with respect to the iron nominal content for all samples. This figure also shows lines which are linear fits to the data for each series of samples. In general, there is a tendency of lattice contraction with increasing iron content for all samples. Two comments should be added here. First, the data for samples annealed at 500 °C are more scattered in comparison to the data for samples annealed at other temperatures. In spite of this scatter, there is a tendency of contraction with increasing iron content. Second, for samples annealed at 650 °C, this contraction only goes up to $x=0.05$, and from that value on the lattice expands suggesting a solubility limit for Fe in SnO_2 at this annealing temperature. The lattice contraction with increasing iron content has also been reported by Punnoose *et al.*,[18] who annealed at 600 °C, but they used another chemical route with iron for tin substitution up to $x=0.05$. If trivalent iron replaces tetravalent tin in the crystallographic structure, then charge balance requires one oxygen vacancy per two irons in the lattice. If we assume that these are the only type of defects present in the samples, then we should expect similar lattice contraction with increasing iron content for all samples. However, it is clearly observed from Fig. 5 that samples do not exhibit similar contraction rates but they depend on the annealing temperature. In order to better explain the variation of the unit cell parameters and lattice volumes we should consider the chemical formula of the samples, which can be generally written as

$$Sn^{4+}{}_{1-x}Fe^{3+}{}_{x}Sn^{2+}{}_{iy}O^{2-}{}_{2-(\delta x+\delta i+\delta')}\square_{(\delta x+\delta i+\delta')}. \quad (1)$$

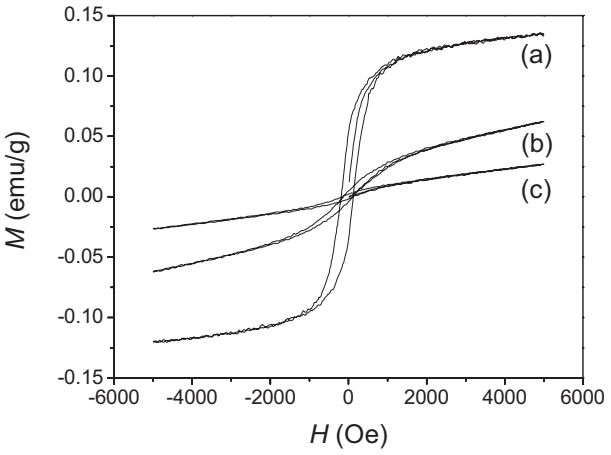

FIG. 6. Room temperature hysteresis loops for $Sn_{0.9}Fe_{0.1}O_{2-\delta}$ samples prepared from (a) HCl solutions of $^{57}Fe_2O_3$ and annealed at 600 °C for 6 h, (b) citric acid solutions of metal ^{57}Fe and annealed at 500 °C for 2 h, and (c) citric acid solutions of metal ^{57}Fe and annealed at 650 °C for 2 h.

The ionic radii for O^{2-}, Sn^{4+} and Fe^{3+} are 0.140, 0.083 and 0.069 nm, respectively. This formula considers that Fe^{3+} is replacing Sn^{4+} in SnO_2. The presence of tin interstitial (Sn^{2+}_i) is also taken into account,[26] although its concentration should be very small or even absent in order to explain the low conductivity often measured in un-doped SnO_2.[27–29] In fact, we collected ^{119}Sn Mössbauer spectra for similar samples (spectra not shown) and we could not detect the presence of Sn^{2+}. The reasons for the Sn^{2+} absence are perhaps due to that the ionic radius of Sn^{2+} is very large than that of Fe^{3+} and Sn^{4+}, and the annealing atmosphere is oxidative in our case. Therefore, the oxygen vacancies ($\square$) are mainly associated to the presence of Fe^{3+} (δy) and to a nonstoichiometric factor (δ'). The presence of these defects changes the O-Sn bond lengths and O-Sn-Sn bond angles, thus increasing the lattice distortion. Therefore, it is highly probable that our samples are nonstoichiometric and contain the defects explained in the chemical formula, thus explaining the behavior of the unit cells and lattice volume parameters.

As shown in Fig. 6, the magnetization, M, versus magnetic field, H, curve for the samples consist of a linear paramagnetic component and a magnetic hysteresis loop. The observed hysteresis loops indicates that some samples are ferromagnetic at room temperature. The contributions of the paramagnetic and ferromagnetic phases were separated after fitting the demagnetization part of the M versus H curves with the function[9,30]

$$M = (2M_s/\pi)(\tan^{-1}\{[(H+H_c)/H_c]\tan(\pi M_r/2M_s)\}) + \chi H, \quad (2)$$

where the first term is the usual function used to represent a ferromagnetic hysteresis curve and the second one is a linear component representing a possible paramagnetic contribution. M_s is the saturation magnetization for the ferromagnetic component, H_c is the coercivity, M_r is the remanent magnetization, and χ is the susceptibility of the paramagnetic component. The parameters derived from the fitting procedure for some samples are listed in Table II. It is important to mention that we do not report the M_s values in Bohr magnetons units per iron ion because, as is discussed below, we believe that the magnetization has different sources, and it is difficult to separate the contribution of each one. Moreover, the magnetic iron ions seem not to be the main source of ferromagnetism in some of our samples. Figure 7 shows a 3D diagram of the variation of M_s with both iron nominal content and annealing temperature. It is possible to see that only under very limited synthesis conditions, room tempera-

TABLE II. Magnetic parameters derived from the fit of the M vs H curves using Eq. (1) for some selected samples. Some information obtained from their Mössbauer spectra is also presented. It is worth recalling that samples annealed at 500 °C and 650 °C were prepared from citric acid solutions of metal ^{57}Fe, whereas those annealed at 600 °C were prepared from HCl solutions of Fe_2O_3.

	500 °C 2 H			600 °C 6 H			650 °C 2 H		
X	0.05	0.1	0.15	0.06	0.1	0.15	0.05	0.1	0.15
M_s (emu/g)	0.3×10^{-4}	4.1×10^{-2}	3.9×10^{-4}	7.1×10^{-4}	12.0×10^{-2}	7.6×10^{-4}	3.0×10^{-4}	1.1×10^{-2}	3.0×10^{-4}
H_c (Oe)	270	264	296	210	193	314	248	426	256
M_r (emu/g)	1.7×10^{-4}	7.7×10^{-3}	0.9×10^{-4}	2.1×10^{-4}	50.0×10^{-3}	2.5×10^{-4}	0.5×10^{-4}	4.5×10^{-3}	0.5×10^{-4}
χ (emu/g/Oe)	3.3×10^{-8}	5.7×10^{-6}	5.6×10^{-7}	2.1×10^{-7}	2.9×10^{-6}	2.0×10^{-7}	4.8×10^{-8}	3.8×10^{-6}	4.8×10^{-8}
RT Mössbauer Components	2 doublets	2 doublets	2 doublets	2 sextets 2 doublets	2 sextets 2 doublets	2 sextets 2 doublets	2 sextets 2 doublets	2 sextets 2 doublets	2 sextets 2 doublets
D1/D2	3.6	4.9	3.5	2	3.1	2.3	2.7	3.7	3

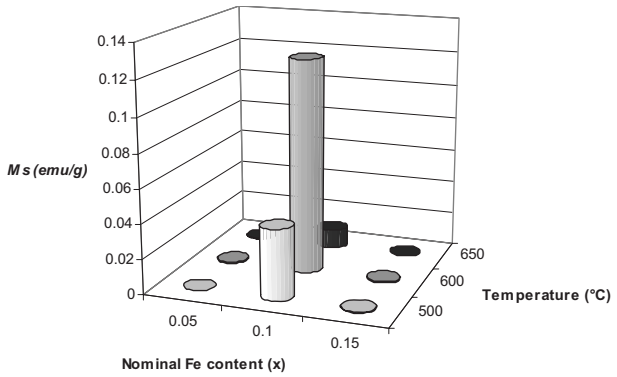

FIG. 7. M_s versus iron nominal content and annealing temperature for some selected samples. Samples annealed at 500 °C and at 650 °C, both for 2 h, come from citric acid solutions of metal ^{57}Fe, whereas sample annealed at 600 °C for 6 h was prepared from HCl solutions of $^{57}Fe_2O_3$.

ture ferromagnetism appears. Thus crystallinity seems not to be directly related to ferromagnetism. Moreover, at the annealing temperature of 650 °C in comparison to that at 500 °C, ferromagnetism is reduced. It is worth mentioning that, Punnoose *et al.*[18] reported a very good correlation between decreasing lattice cell volume and increasing magnetization suggesting strong structure-magnetic property relationship in their samples, which were prepared using a different chemical method and for iron concentrations less than 0.05. Clearly this is not the case in our samples, suggesting that the preparation method affects the properties of the final products, and that at lower iron concentrations ($x \leqslant 0.05$) the behavior of magnetization and crystallinity is more regular. Inaba *et al.*[31] have also reported very restricted experimental conditions for ferromagnetism to appear in Fe doped TiO_2 thin films.

Typical room temperature Mössbauer spectrum for sample $x=0.1$ annealed at 500 °C is shown in Fig. 8(c). The spectrum is properly fitted with two doublets. The necessity of a second doublet is clearly seen in the small shoulder of the main doublet located at the low velocity side of the spectra. It is important to mention that Coey *et al.*[15] and Punnoose *et al.*[18] used only one doublet and one sextet to fit their Mössbauer spectrum. However, Punnoose *et al.*[18] did not use ^{57}Fe enriched samples, and Coey *et al.*[15] used ^{57}Fe enriched thin films in transmission Mössbauer spectra instead of CEMS. Our spectra are better resolved than those presented in their papers. For samples with $x<0.05$ an additional relaxed sextet is observed whose relative intensity increases with decreasing Fe doping (see Table III).

From the analysis of the Mössbauer spectra of all samples annealed at 500 °C we found that doublet 1 (D1) shows center shifts, δ, in the range of $0.36\ \text{mm/s} < \delta < 0.37\ \text{mm/s}$ and quadrupole splittings, Δ, in the range of $0.69\ \text{mm/s} < \Delta < 0.83\ \text{mm/s}$, whereas doublet 2 (D2) exhibits $0.27\ \text{mm/s} < \delta < 0.35\ \text{mm/s}$ and $1.56\ \text{mm/s} < \Delta < 2.07\ \text{mm/s}$ (see Table III). These parameters suggest that all the iron ions are high spin 3+, and that the former and the latter Fe species are located in octahedral sites without and with oxygen vacancy, respectively. Thus Fe is replacing Sn in the SnO_2 structure in good agreement with XRD and SEM

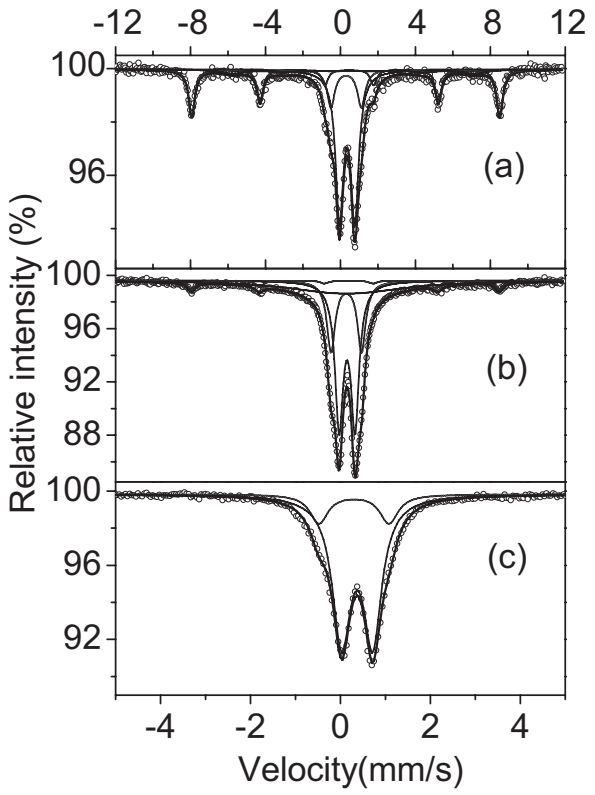

FIG. 8. Room temperature Mössbauer spectra of $Sn_{0.9}Fe_{0.1}O_{2-\delta}$ samples prepared from (a) citric acid solutions of metal ^{57}Fe and annealed at 650 °C for 2 h, (b) HCl solutions of $^{57}Fe_2O_3$ and annealed at 600 °C for 6 h, and (c) citric acid solutions of metal ^{57}Fe and annealed at 500 °C for 2 h.

data. More specifically, we believe that possible iron site paths are

$$Sn^{4+} - O^{2-} - Fe^{3+} - O^{2-} - Sn^{4+}, \quad (3)$$

$$Sn^{4+} - O^{2-} - Fe^{3+} - \square - Sn^{4+}, \quad (4)$$

$$Sn^{4+} - O^{2-} - Fe^{3+} - \square - Fe^{3+}, \quad (5)$$

$$Sn^{4+} - \square - Fe^{3+} - O^{2-} - Fe^{3+}, \quad (6)$$

$$Sn^{4+} - \square - Fe^{3+} - \square - Sn^{4+}. \quad (7)$$

Thus there are some iron ions located close to oxygen vacancies, □, and others that are not. We propose that doublet D1, with the lowest quadrupole splitting values and thus less distorted sites, originate from irons far from defects (see path number 3), and doublet D2, with the largest quadrupole splitting values and thus more distorted sites, come from those iron close to the defects (see path numbers 4 to 7). We have found that the D1/D2 area ratio is always greater than 3.9, and has the largest value of 4.9 for sample $x=0.1$ (see Table II). In other words, there are more D1 sites than D2 sites, which mean that there are more irons far from defects than those close to it, if our iron site assignments are correct. This means that either iron does not prefer to stay close to the defects or that there are few of them in the lattice. This result

TABLE III. Hyperfine parameters obtained from the fit of the room temperature Mössbauer spectra for those samples prepared from citric acid solutions of metal ^{57}Fe and annealed at 500 °C for two hours. Estimated errors are of about ±0.01 mm/s for the isomer shift, δ, quadrupole splitting, Δ, quadrupole shift, 2ε, and linewidth, Γ, of about ±0.2 T for the average magnetic hyperfine field, $\langle B\rangle$, and of about ±2% for the relative area, A. D1 and D2 are for doublet 1 and 2, respectively.

x		0.005	0.01	0.03	0.05	0.1	0.15
	δ (mm/s)	0.37	0.37	0.37	0.36	0.37	0.36
	Δ (mm/s)	0.76	0.75	0.77	0.83	0.69	0.78
D1	Γ (mm/s)	0.80	0.64	0.66	0.79	0.49	0.58
	A (%)	50	58	60	69	83	78
	δ (mm/s)	0.35	0.31	0.30	0.27	0.30	0.30
	Δ (mm/s)	2.07	1.72	1.68	1.80	1.56	1.61
D2	Γ (mm/s)	0.80	0.64	0.66	0.79	0.49	0.58
	A (%)	14	15	14	19	17	22
	δ (mm/s)	0.69	0.31	0.31	0.64		
	2ε (mm/s)	0.01	0.01	0.01	0.01		
Sextet	$\langle B\rangle$ (T)	27.3	13.0	10.9	20.6		
	A (%)	36	27	26	12		

TABLE IV. Hyperfine parameters obtained from the fit of the 10 K Mössbauer spectra for those samples prepared from citric acid solutions of metal ^{57}Fe and annealed at 500 °C for two hours. Estimated errors are of about ±0.01 mm/s for the isomer shift, δ, quadrupole splitting, Δ, quadrupole shift, 2ε, and linewidth, Γ, of about ±0.1 T for the average magnetic hyperfine field, $\langle B\rangle$, and of about ±2% for the relative area, A. D1 and D2 are for doublet 1 and 2, respectively.

x		0.01	0.03	0.05	0.1
	δ (mm/s)	0.41	0.46	0.45	0.48
	Δ (mm/s)	0.48	0.76	0.67	0.69
D1	Γ (mm/s)	0.68	0.68	0.68	0.61
	A (%)	38	59	49	81
	δ (mm/s)	0.45	0.41	0.43	0.40
	Δ (mm/s)	1.31	1.78	1.67	1.31
D2	Γ (mm/s)	0.68	0.68	0.68	0.61
	A (%)	22	22	31	19
	δ (mm/s)	0.49	0.45	0.47	
	2ε (mm/s)	−0.1	−0.11	0	
Sextet	$\langle B\rangle$ (T)	50.2	50.5	47.5	
	A (%)	41	20	20	

seems to be at odds with theoretical calculations by Errico *et al.*[32] in Fe doped TiO_2, which states that iron prefers to be located close to oxygen vacancy sites. It is considered that carrier or itinerancy electrons are related with the far defect because SnO_{2-x} is semiconductor. The incorporated Fe^{3+} and oxygen vacancy of SnO_2 is considered to have low energy of formation and strongly mutual attraction even at the long distance.

We have observed that the magnetization curves for samples $x=0.1$ and 0.15 annealed at 500 °C appear to be contrary to their room temperature Mössbauer spectra, because they exhibit the largest saturation magnetization values among the samples annealed at this temperature but they do not show sextets. This discrepancy has also been reported for $Ti_{1-x}Fe_xO_{2-\delta}$[33] and $Zn_{1-x}Fe_xO_{1-\delta}$,[34] and explained by the effect of interaction between the host lattices and the spins of the doped Fe ions from the relaxation phenomena, i.e., a paramagnetic spin-lattice relaxation. We do not believe this explanation can be used here to understand the discrepancy, because there are some samples that exhibit the opposite tendency, i.e., a sextet is clearly visible and they exhibit weak magnetization. Moreover, there are some samples exhibiting weak magnetization and showing weak relaxed sextets (samples with $x<0.05$ annealed at 500 °C). Additionally, if this model is correct then we should expect a great change in the Mössbauer spectra at low temperatures, where this relaxation should be greatly reduced. We have collected 10 K Mössbauer spectra for some samples annealed at 500 °C. The low temperature and room temperature spectra were fitted similarly, i.e., we used two doublets and/or one sextet, and the derived hyperfine parameters for the spectra at 10 K are presented in Table IV. Except for the sample with $x=0.01$, there is no significant growth of the magnetic sextet relative area with decreasing temperature, but the area of doublet D2 increases at expenses of doublet D1. Moreover, the spectrum for sample $x=0.1$ does not exhibit a sextet. On the other hand, as will be shown below, the low temperature spectra for sample $x=0.1$ prepared from HCl solutions of $^{57}Fe_2O_3$ and annealed at 600 °C, show also similar features. Similar behavior of the low temperature Mössbauer spectra for ceramic Fe doped SnO_2 samples were reported by Fitzgerald *et al.*[16] Thus it is clear that we need another explanation to the discrepancy, and this will be given in the Discussion section.

The room temperature Mössbauer spectrum for sample $x=0.1$ annealed at 650 °C is shown in Fig. 8(a). The spectrum is properly fitted by introducing two doublets, one weak relaxed sextet and one sextet with sharp lines. The latter sextet is required for samples with $x>0.03$. The derived parameters are listed in Table V. From the analysis of the data we found that, for doublet 1, 0.35 mm/s $<\delta<$ 0.36 mm/s and 0.81 mm/s $<\Delta<$ 0.96 mm/s; whereas for doublet 2, 0.30 mm/s $<\delta<$ 0.34 mm/s and 1.60 mm/s $<\Delta<$ 2.31 mm/s. The assignments of the doublets and the relaxed sextet are the same as for samples annealed at 500 °C. We have found that the D1/D2 area ratio is always greater than 2.1 (see Table II). On the other hand, the relative intensity of the sharp sextet increases with increasing Fe doping, and can accounts for almost 50% of the relative area in sample $x=0.15$. This sharp sextet was not observed in the samples annealed at 500 °C. The parameters of the sextet with relatively sharp lines ($\delta=0.38$ mm/s; $\Delta=-0.18$ mm/s; $B_{hf}=51$ T) are really very similar to that of α-Fe_2O_3.[11] For comparison purposes, the magnetization values for all samples annealed at 650 °C are negligible. α-Fe_2O_3 shows weak ferromagnetism at room temperature.

TABLE V. Hyperfine parameters obtained from the fit of the room temperature Mössbauer spectra for those samples prepared from citric acid solutions of metal ^{57}Fe and annealed at 650 °C for two hours. Estimated errors are of about ±0.01 mm/s for the isomer shift, δ, quadrupole splitting, Δ, quadrupole shift, 2ε, and linewidth, Γ, of about ±0.2 T for the average magnetic hyperfine field, $\langle B \rangle$, and of about ±2% for the relative area, A. D1 and D2 are for doublet 1 and 2, respectively.

x		0.005	0.01	0.05	0.1	0.15
	δ (mm/s)	0.36	0.35	0.35	0.36	0.36
	Δ (mm/s)	0.91	0.87	0.96	0.81	0.84
D1	Γ (mm/s)	0.82	0.71	0.75	0.49	0.49
	A (%)	52	66	60	55	36
	δ (mm/s)	0.34	0.30	0.30	0.31	0.31
	Δ (mm/s)	2.31	1.86	1.79	1.60	1.60
D2	Γ (mm/s)	0.82	0.71	0.75	0.49	0.49
	A (%)	10	19	23	15	12
	δ (mm/s)	0.57	0.39	0.39	0.67	0.45
	2ε (mm/s)	0.13	0	0.02	0.03	0.02
Sextet 1	$\langle B \rangle$ (T)	31.5	6.0	12.4	39.9	27.0
	A (%)	38	16	16	9	8
	δ (mm/s)			0.37	0.38	0.38
	2ε (mm/s)			51.0	51.0	51.0
Sextet 2	$\langle B \rangle$ (T)			–0.19	–0.18	–0.20
	A (%)			16	27	48

In order to investigate the effect of annealing time on the magnetic properties, samples with $x=0.1$ and 0.15 prepared using citric acid solutions of metal ^{57}Fe were annealed at 500 °C for 2 and 6 h. Figure 9 shows the magnetization versus applied field curves for sample $x=0.1$. It is clearly shown that the hysteresis is greatly reduced with annealing time, and that M_s reduces from 0.038 emu/g to 0.015 emu/g. The reduction of M_s is less pronounced for sample with $x=0.15$. On the other hand, M_r decreases and H_c increases with annealing time. The insets in Fig. 9 also show the corresponding room temperature Mössbauer spectrum, which consist only of two doublets with similar hyperfine parameters to the ones reported above. The area ratio of D1/D2 (see last row in Table II) is slightly reduced for sample $x=0.1$ but remains the same for sample $x=0.15$ with increasing annealing time. Clearly the annealing process in the presence of air has a strong influence upon the magnetic properties of the final products. With the increment of the time for the thermal treatment, the number of iron ions remains the same but we expect less oxygen vacancies, thus oxygen vacancies must be taken into account as an important source of ferromagnetism.

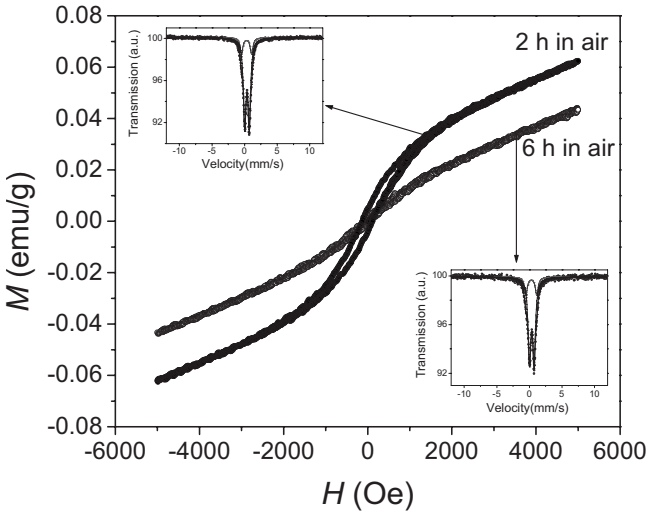

FIG. 9. Hysteresis loops for $Sn_{0.9}Fe_{0.1}O_{2-\delta}$ samples prepared from citric solutions of metal ^{57}Fe and annealed at 500 °C for 2 h and 6 h in air. The insets show their respective room temperature Mössbauer spectra.

B. Samples prepared from HCl solutions of $^{57}Fe_2O_3$ and annealed at 600 °C for 6 h

The color of the samples changed from pale gray for samples with low and medium iron contents to light yellow-orange for samples with the higher iron contents. From Table I, it is noticed that the measured EDAX concentrations are in reasonable agreement with their nominal compositions. Figure 10 shows SEM micrographs for some selected samples. At low iron doping larger particles with irregular shapes are formed, but as iron content increases the particles start to exhibit fine grained sandy type morphology. Figure 1 demonstrates that the particle size decreases with increasing Fe doping, in agreement with the behavior reported for the samples prepared from the ^{57}Fe metal solutions.

The XRD patterns were fitted by introducing only the cassiterite phase of SnO_2. Very weak hematite peaks were also observed for those samples having the higher iron contents. On the other hand, the a and c lattice parameters are observed to increase and decrease with increasing iron content respectively (see Fig. 4). The lattice volume also decreases with increasing iron nominal content, also the rate is different in comparison to the other samples (see Fig. 5). Explanations of all these observations were provided above by using the chemical formula number (1).

In relation to the magnetization results, the largest M_s values of 0.12 and 0.04 emu/g were obtained for samples with $x=0.1$ prepared using HCl solutions of $^{57}Fe_2O_3$ and annealed at 600 °C for 6 h and also using citric acid solutions of ^{57}Fe metal and annealed at 500 °C for 2 h, respectively (see Fig. 7 and Table II). For comparison purposes, Punnoose *et al.*[18] have reported a maximum value of 0.035 emu/g for a synthetic sample with $x=0.05$ annealed at 600 °C using another chemical route. Coey *et al.*[15] found larger moments in Fe-doped thin films when the films were grown from ceramic targets made of FeO and SnO_2 instead of Fe_2O_3 and SnO_2. All these results suggest that the starting materials seem to play an important role in the final ferromagnetic properties of the products.

The room temperature spectrum for sample $x=0.1$ is presented in Fig. 8(b). The same components but with different

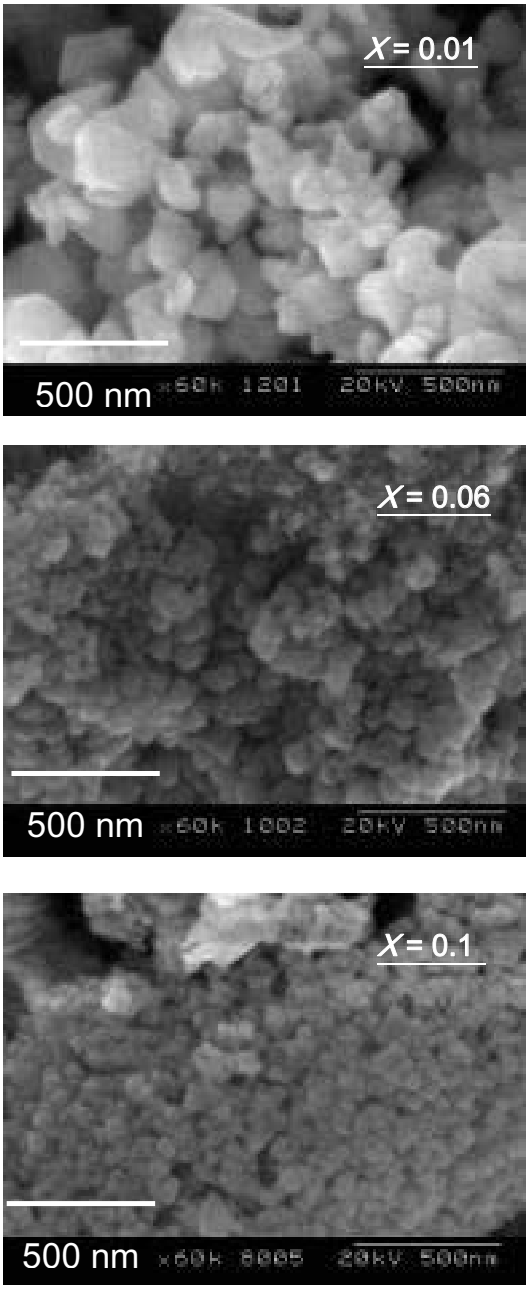

FIG. 10. SEM micrographs of some selected $Sn_{1-x}Fe_xO_{2-\delta}$ samples prepared from HCl solutions of $^{57}Fe_2O_3$ and annealed at 600 °C for 6 h.

relative intensities were observed as for the spectra of sample $x=0.1$ prepared from citric acid solutions of ^{57}Fe metal and annealed at 650 °C for 2 h. The data derived from the analysis of the Mössbauer spectra of samples annealed at 600 °C are presented in Table VI. We found that, for doublet 1, 0.35 mm/s $<\delta<$ 0.47 mm/s and 0.81 mm/s $<\Delta<$ 0.96 mm/s; whereas for doublet 2, 0.29 mm/s $<\delta<$ 0.38 mm/s and 1.56 mm/s $<\Delta<$ 2.09 mm/s. The sextet with sharp lines starts to appear for samples with $x>0.06$. For $x=0.1$ the relative area of this sharp sextet accounts only about 6%. On the other hand, we found that the D1/D2 area ratio is always greater than 2, and has the largest value of 3.1 for sample $x=0.1$ at all annealing temperatures. It is interesting to mention that samples with $x=0.1$ have the largest M_s and D1/D2 values.

TABLE VI. Hyperfine parameters obtained from the fit of the room temperature Mössbauer spectra for those samples prepared from chloride acid solutions of $^{57}Fe_2O_3$ and annealed at 600 °C for six hours. Estimated errors are of about ±0.01 mm/s for the isomer shift, δ, quadrupole splitting, Δ, quadrupole shift, 2ε, and linewidth, Γ, of about ±0.2 T for the average magnetic hyperfine field, $\langle B\rangle$, and of about ±2% for the relative area, A. D1 and D2 are for doublet 1 and 2, respectively.

x		0.01	0.02	0.06	0.1
	δ (mm/s)	0.47	0.35	0.36	0.36
	Δ (mm/s)	0.94	0.81	0.83	0.81
D1	Γ (mm/s)	0.86	0.56	0.53	0.70
	A (%)	44	49	46	40
	δ (mm/s)	0.38	0.29	0.32	0.31
	Δ (mm/s)	2.09	1.72	1.57	1.56
D2	Γ (mm/s)	0.86	0.56	0.53	0.70
	A (%)	18	17	23	12
	δ (mm/s)	0.37	0.42	0.37	0.39
	2ε (mm/s)	0	0	0.03	0.04
Sextet 1	$\langle B\rangle$ (T)	24.8	11.8	25.1	25.7
	A (%)	37	34	26	41
	δ (mm/s)			0.35	0.37
	2ε (mm/s)			50.9	51.1
Sextet 2	$\langle B\rangle$ (T)			−0.20	−0.20
	A (%)			6	6

IV. DISCUSSION

A. General aspects

In relation to the synthesis conditions, our results seems to suggest that (i) the starting solutions affect the annealing time required for the formation of Fe doped SnO_2 powders, (ii) the annealing time affects the concentration of defects and possibly the crystallographic rearrangement, and (iii) the annealing temperature affects the degree of homogeneity of the irons in the particles. Let us explain one by one in more detail.

(i) *Starting solutions*. In our samples, we used the same Sn solution but two different iron solutions. At the beginning we thought that the starting iron solution should not have any influence in the experiments. However, it did affect the annealing time, which depended on the color change from black (for the bulk polymeric complex) to pale gray (for the final Fe doped SnO_2 powder). We found that this color change was achieved after two hours of annealing for those samples coming from the citric acid solutions of dissolved metal ^{57}Fe, but after 6 h of annealing for those samples containing chloride acid solutions of dissolved $^{57}Fe_2O_3$. A possible explanation for this increment in the annealing time is that the chloride ions, which are more concentrated in the

solutions $^{57}Fe_2O_3$, required longer times to be evaporated. Thus, while the Cl ions are evaporated, the powders have to their disposal thermal energy and oxygen for longer periods of time, allowing crystallographic rearrangement and reduction in the number of defects, respectively.

(ii) *Annealing time*. As shown in Fig. 9, we have found that the magnetization is greatly reduced with increasing the annealing time. We expected that with the increment of thermal treatment time, the number of iron ions remain the same, but the concentration of oxygen vacancies and possibly the tin interstitial be reduced. Thus, annealing time seems to affect the number of oxygen vacancies (point defects), which must be taken into account as an important source of ferromagnetism as explained below.

(iii) *Annealing temperature*. At lower temperatures the iron ions distribute more homogeneously in the whole particle, but with increasing temperature, the iron tends to diffuse towards the surface. This interpretation is supported by our EDAX study and also by the reports by Punnoose *et al.*[18] and by Davis *et al.*[22]

Now, let us concentrate upon the interpretation of the observed magnetic properties. The presence of iron impurities and various types of defects must be taken into account. Moreover, Mössbauer results show that samples exhibit atomic scale inhomogeneity in the magnetic iron ions, some of them belonging to isolated sites, and others to magnetically interacting ones. A highly controversial issue in doped DMS materials is the origin of ferromagnetism. It has been reported that cobalt clustering can cause room-temperature ferromagnetism in the Co-doped TiO_2 anatase films,[35] and that Fe_3O_4 can do the same in Fe-doped TiO_2 rutile films.[36] Kundaliya *et al.*[25] found that the observed ferromagnetism in the low-temperature processed Mn-Zn-O system is due to the formation of an oxygen-vacancy-stabilized $Mn_{2-x}Zn_xO_{3-\delta}$. Thus, considering this controversy, we need to be sure that our samples do not contain traces of metallic iron clusters, magnetite, or magnetite. First of all, Rietveld analysis of the XRD patterns plotted in log scale and in some expanded regions did not show the presence of any iron compound, except with the high iron contents and high annealing temperatures. This method has been successfully used to provide the presence[25] or absence[18] of small traces of impurity phases. On the other hand, we have used enriched ^{57}Fe samples and one iron compound with a relative area abundance of 1–2 % can be detected by Mössbauer spectroscopy. This means that 0.11–0.21 wt. %, or 0.11–0.21 % in mass of any iron compound in SnO_2 should be detected. However, within this resolution limit, we could not see any sextet component due to impurity phases. Moreover, for some samples [see Fig. 8(b)], the room temperature Mössbauer spectrum clearly shows the presence of one sextet which accounts for 42% of the relative area. The shape of the low temperature Mossbauer spectra down to 10 K for the same sample did not change as much as expected if we had magnetite. In fact, below the Verwey transition, T_v, of about 120 K, the Mössbauer spectrum of magnetite becomes more complex changing from two sextets (above T_v) to five sextets (below T_v).[37] Now, the color of none of our samples is somehow black or dark brown as expected if minor amounts of magnetite and maghemite impurities are formed, respectively. On the other hand, Punnoose *et al.*,[18] reported that using a sol-gel method maghemite could be formed at 200 °C, but not in the range of 350–600 °C, and Davis *et al.*[22] reported the possible formation of magnetite only above 900 °C. The sol-gel method in conjunction with the drying and annealing process in air intrinsically eliminates the possibility of forming metallic iron. Moreover, under these oxidizing conditions the formation of Fe^{2+} ions is greatly reduced or even ruled out, and thus the formation of magnetite. For all those reasons, we believe that ferromagnetism in our samples is an intrinsic property and not due to the presence of minor iron phase impurities.

Punnoose *et al.*[18] have suggested that changes in the internal or external lattice volume or pressure should be considered as a possible source of ferromagnetism. This hypothesis is usually based upon the experimental fact that saturation magnetization and lattice volume are closely related. However, this model cannot be used in our samples because we did not find any connection between magnetism and crystallinity. In fact, there is a smooth variation in the lattice volume (see Fig. 5) for a given series of samples, but on the contrary, there is a sharp increase in the M_s values (see Fig. 7) for certain iron concentrations.

The source of the observed magnetism seems to be different for each sample. We will discuss here the origin of the magnetic ordering for the most interesting ones, i.e., those with $x=0.1$, which exhibit the highest M_s values (see Fig. 7).

B. Magnetism in the sample prepared from citric acid solution of metal ^{57}Fe annealed at 500 °C for 2 h

As shown above (see Sec. III A), the magnetic impurities seem not to contribute to the observed magnetism, because the Mössbauer spectrum for this sample does not show sextets even at lower temperatures. To explain the lack of magnetic signal originating from the iron ions we can take into consideration the following two arguments. First of all, the sol-gel method produces a homogeneous distribution of the iron ions in the lattice. This interpretation is supported by our EDAX study and also by the reports by Punnoose *et al.*[18] and by Davis *et al.*[22] The second aspect is that at 500 °C, which was the lowest temperature used for annealing the samples, in comparison to 650 °C, the iron ions are more homogeneously distributed in the entire particle. However, with increasing temperature they tend to diffuse and accumulate toward the surface. Thus longer iron-iron distances are expected in the samples annealed at 500 °C than at 650 °C, thus reducing the iron-iron interactions mediated by either oxygens or by electrons trapped at vacancies. This can be one of the reasons for the lack of magnetic signal originating from the iron ions. Thus, we have to look for another source of the magnetic signal. Coey and co-workers[1,8] have reported that some point defects like F_t or V^0 centers can order ferromagnetically in Co or Sc doped ZnO. They, when discussing the nature of the defects in oxides DMS, recognized that the electron defects may themselves form an impurity band that could split spontaneously if narrow enough or be polarized by exchange with $3d$ cations. Elfimov *et al.*[6] reported that cation vacancies in undoped CaO can order ferromagneti-

cally. Monnier and Delley[38] have also reported that anion vacancies in CaB_6 can order ferromagnetically. Bouzerar and Ziman[39] recently have proposed a model for vacancy-induced ferromagnetism in oxides and applied it to explain the magnetic behavior of undoped ZrO_2, HfO_2, and CaO. Thus there are theoretical and experimental evidence that the defects can become magnetically ordered and may become the main or the only source of magnetism. Thus it seems that the defects in our sample are responsible not only for providing the *n*-type conduction, but perhaps to be an important source of ferromagnetism too. In fact, XRD and SEM results suggest that this sample contains different concentration of defects in comparison to the other samples. Possible defects presented here are: oxygen vacancy, tin interstitial, iron interstitial, tin antisite, iron antisite, tin vacancy, oxygen interstitial. The substitution of tin by iron is a defect itself that creates another oxygen vacancy because of charge balance requirement. Based upon the work by Kilic and Zunger,[26] only tin interstitial and oxygen vacancy are the most probable defects in undoped samples. Now, the concentration of tin interstitial and related oxygen vacancy defects in our samples should be very small or even absent; otherwise, we should be able to notice SnO-like fingerprints in the XRD patterns and/or ^{119}Sn Mössbauer spectrum, which were not observed. Now in our Fe doped SnO_2, we do not believe we have interstitial iron, otherwise we should expect a doublet in the Mössbauer spectra with different parameters, especially in the isomer shift, which is not seen. Thus, in summary we have a nonstoichiometric Fe doped SnO_2, which contains Fe^{3+} and two types of O^{2-} vacancies. The first type is an oxygen vacancy required by the replacement of Sn^{4+} by Fe^{3+}, whereas the second one comes from a nonstoichiometric factor, as explained in the chemical formula (1). The oxygen vacancies can trap one or two electrons, and it is probable that we have ferromagnetically ordered point defects like F_t centers, which consist of two adjacent singly occupied vacancies (F centers).[40] These defects have low-lying triplet states, which can form an impurity band that can be polarized by exchange with Fe^{3+} ions. We would like to comment that we do not believe that Sn^{3+} can explain the observed magnetism because this is not a stable oxidation state, and it is not common in this sample as reported in different works.[26] Additionally, we propose that the absence of Fe-vacancy-Fe magnetic polarons are due to the fact that oxygen vacancies prefer to be located far to the iron impurities as we have found through the D1/D2 area ratio. Finally, we want to mention that Fitzgerald *et al.*[41] have recently proposed another type of magnetic defect: O_2^{2-} peroxide ions linking adjacent octahedral, each of which is occupied by Fe^{3+} ion. Two oxygen vacancies separated by a cation vacancy, named the trivacancy system, is also another source of magnetic defect.[40] However, Kilic and Zunger[26] have demonstrated that tin vacancies are very improbable. More experiments and theoretical research are required to solve this issue.

C. Magnetism in the sample prepared from HCl solutions of $^{57}Fe_2O_3$ annealed at 600 °C for 6 h

Coey *et al.*[1,15] proposed a ferromagnetic coupling of ferric ions via an electron trapped in a bridging oxygen vacancy.

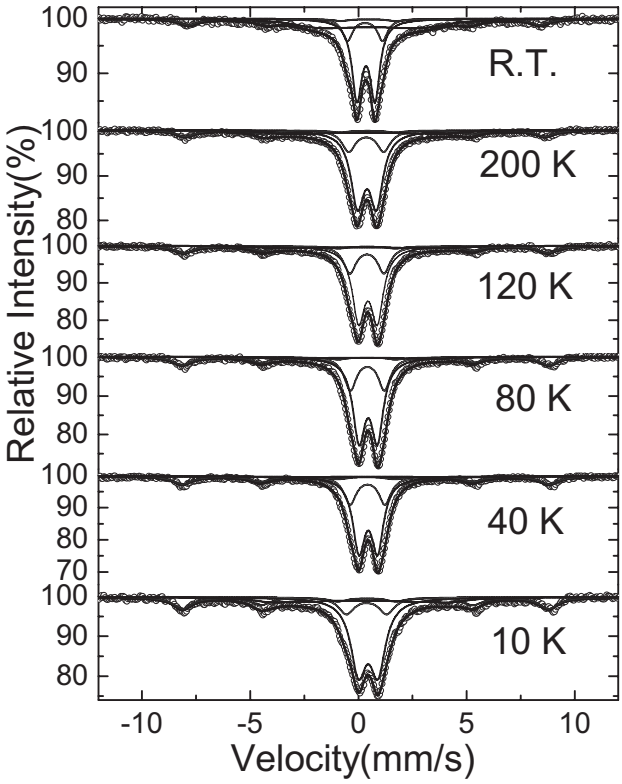

FIG. 11. Low temperature Mössbauer spectra of $Sn_{0.9}Fe_{0.1}O_{2-\delta}$ sample prepared from HCl solution of $^{57}Fe_2O_3$ and annealed at 600 °C for 6 h.

By using their model, we found that this sample is below the cation percolation threshold, x_p, associated with nearest neighbor cation coupling and also above the donor polaron percolation threshold, δ_p, associated with the ferromagnetic exchange mediated by shallow donor electrons that form bound magnetic polarons. In fact, the iron concentrations, x, ranges from 0 to 0.15, and according to the magnetic phase diagram for dilute magnetic semiconductors $x_p > 0.2$, thus $x < x_p$. On the other hand, according to Coey *et al.*[1] $\delta_p \sim 0.001$, and using their chemical formula of $(Sn_{1-x}Fe_x) \times (O\square_{\delta'})_2$ and taking into consideration only charge balance for iron then $0.00125 < \delta' < 0.0375$. Of course if we include tin interstitial defects, more oxygen vacancies are formed, thus increasing the value of δ'. Therefore, we have $\delta' > \delta_p$ and that $x < x_p$, thus ferromagnetic interaction is expected in our samples. The room temperature Mössbauer spectrum for this sample exhibits a relaxed sextet with a relative area of about 42%. By comparison, Coey *et al.*[15] and Punnoose *et al.*[18] reported a relative area value of about 23% for the sextet component, whereas Fitzgerald *et al.*[16] obtained a value of 86%. In these works, the sextet did not exhibit magnetic relaxation behavior. In order to investigate in more detail the origin of this relaxed sextet in our sample, we have collected Mössbauer spectra at lower temperatures down to 10 K. The spectra were fitted in the same way as the room temperature one and the results are shown in Fig. 11. It is possible to see that the shape of the spectra did not noticeably change with respect to the room temperature one. These data suggest that relaxation can be originated from weakly

interacting magnetic polarons or small size polaron clusters.

It is important to mention that the room temperature ferromagnetism for this sample can also have other different sources. Janisch and Spaldin[42] proposed that ferromagnetic ordering can also originate from superexchange interaction between magnetic moments of neighboring transition metal dopants that shows a 90° metal-anion-metal bond. On the other hand, based upon the fact that agreement between a combination of first principles calculations and simulation on the one hand and experiment on the other hand is only achieved when the magnetic ions are randomly distributed in the host lattice, Bergqviast *et al.*[43] have proposed that the magnetic ordering in DMS materials is greatly affected by magnetic percolation, and that the main source of ferromagnetism comes from short ranged interatomic exchange interactions that are strongly localized in real space. Moreover, it is also possible that magnetic defects can be also contributing to the magnetization value. These different sources of ferromagnetism cannot be neglected here, but it is difficult to establish which is the main one or the amount of iron ions that are involved in each type of ordering. Finally, we recall that the Mössbauer spectrum for this sample exhibits a sextet with sharp lines accounting for about 6% relative area, which comes from hematite.

D. Magnetism in the sample prepared from citric acid solution of metal ^{57}Fe annealed at 650 °C for 2 h

The source of the observed magnetism seems to be completely different from the previously mentioned samples. The origin of the sextet with relatively sharp lines is related with the presence of hematite. In fact, we believe that several % of iron oxides are segregated in the surface of SnO_2 grains by heating at high temperatures and forms Sn doped hematite. This interpretation is in agreement with the XRD and color results. Moreover, the weight fraction derived from the Rietveld refinement analysis is in good agreement with the relative abundance derived from the Mössbauer area fractions. Davis *et al.*[22] reported Fe diffusion from the inner core to the outer shell of the particles with increasing temperature, and the formation of Fe_3O_4. Now we propose the presence of hematite doped with tin, because the quadrupole shift at low temperatures for another sample whose hematite relative area accounts for 6% (see Fig. 11), does not greatly differ from the room temperature one. It is well known that quadrupole shift changes from −0.2 mm/s to 0.4 mm/s at 260 K, i.e., the Morin transition, but this variation is not observed in our samples. In fact, Morrish[44] has reported that Sn^{4+} greatly reduces or even destroys the Morin transition in hematite. Therefore, no changes, especially in the quadrupole shift, are expected even at low temperatures as observed in our samples. We would like to mention that Fitzgerald *et al.*[16] and Coey *et al.*[15] reported that Mössbauer spectroscopy is not capable of distinguishing between Sn^{4+} doped hematite and Fe^{3+} doped SnO_2, because they exhibit similar hyperfine parameters. However, we have demonstrated here that by using the complementary quantitative XRD analysis plotted in log scale for some selected expanded regions the presence of hematite can be noticed even if present in minor amounts.

V. CONCLUSIONS

Our results suggest that we are dealing with samples which exhibit very complex ferromagnetism coming from different sources that include not only interaction between ferric ions, but also interaction between magnetic defects. The dominance of a given source of magnetism greatly depends upon synthesis conditions. Sample $x=0.1$ prepared using HCl solution of $^{57}Fe_2O_3$ and annealed at 600 °C for 6 h exhibits ferromagnetism and shows a relaxed sextet in the Mössbauer spectrum, thus the main source of magnetism seems to be related with ordered iron ions. On the other hand, sample $x=0.1$ prepared using citric acid solution of metal ^{57}Fe and annealed at 500 °C for 2 h is also ferromagnetic but its Mössbauer spectrum consists only of doublets with large Δ, thus the main source seems to be related with magnetic defects. Finally, for sample $x=0.1$ prepared using citric acid solution of metal ^{57}Fe and annealed at 650 °C for 2 h, which exhibit an intensive sextet with sharp lines but negligible magnetization, the observed weak magnetism is mainly attributed to the presence of hematite doped with Sn. We have found that the Mössbauer spectra for all samples always show two doublets but for some samples a relaxed magnetic sextet originating from magnetically ordered ferric ions is also observed. For some samples, especially those annealed at 650 °C an additional sextet with sharp lines was attributed to the presence of hematite doped with tin. We have assigned one of the doublets to iron ions substituting tin ions and surrounded by six nearest neighbors oxygen ions, whereas the other doublet comes from those irons also replacing tin but surrounded with at least one oxygen vacancy. The area ratio of the two doublet sites suggests that iron prefers to be located far from the oxygen vacancies or defects. We need to control the annealing temperature and time in a certain atmosphere, depending on the starting reactive agents and iron concentration.

ACKNOWLEDGMENTS

This study was partially supported by Asahi Glass Foundation. One of the authors, C.A.B., is a visiting researcher who is supported by the Matsumae International Foundation. The authors would like to express thanks to T. Ohki and T. Ikeda, Kobelco Research Institute Inc., for help in measuring VSM, and to S. Iio, School of Engineering, The University of Tokyo for help in measuring some Mössbauer spectra.

*Corresponding author.
Electronic address: cbarrero@pegasus.udea.edu.co

[1] J. M. D. Coey, M. Venkatesan, and C. B. Fitzgerald, Nat. Mater. **4**, 173 (2005).
[2] T. Dietl, Semicond. Sci. Technol. **17**, 377 (2002).
[3] R. Janisch, P. Gopal, and N. A. Spaldin, J. Phys.: Condens. Matter **17**, R657 (2005).
[4] H. Ohno, Science **281**, 951 (1998).
[5] W. Prellier, A. Fouchet, and B. Mercey, J. Phys.: Condens. Matter **15**, R1583 (2003).
[6] I. S. Elfimov, S. Yunoki, and G. A. Sawatzky, Phys. Rev. Lett. **89**, 216403-1 (2002).
[7] M. Venkatesan, C. B. Fitzgerald, and J. M. D. Coey, Nature (London) **430**, 630 (2004).
[8] M. Venkatesan, C. B. Fitzgerald, J. G. Lunney, and J. M. D. Coey, Phys. Rev. Lett. **93**, 177206-1 (2004).
[9] S. Duhalde, M. F. Vignolo, F. Golmar, C. Chiliotte, C. E. Rodríguez Torres, L. A. Errico, A. F. Cabrera, M. Rentería, F. H. Sánchez, and M. Weissmann, Phys. Rev. B **72**, 161313(R) (2005).
[10] Y. Matsumoto, M. Murakami, T. Shono, T. Hasegawa, T. Fukumura, M. Kawasaki, P. Ahmet, T. Chikyow, S.-Y. Koshihara, and H. Koinuma, Science **291**, 854 (2001).
[11] K. Nomura, C. A. Barrero, J. Sakuma, and M. Takeda, Czech. J. Phys. **56**, E75 (2006).
[12] K. Nomura, K. Inaba, S. Iio, T. Hitosugi, T. Hasegawa, Y. Hirose, Z. Hommonay, Hyperfine Interact. **168**, 1065 (2006).
[13] H. Kimura, T. Fukumura, M. Kawasaki, K. Inaba, T. Hasegawa, and H. Koinuma, Appl. Phys. Lett. **80**, 94 (2002).
[14] S. B. Ogale, R. J. Choudhary, J. P. Buban, S. E. Lofland, S. R. Shinde, S. N. Kale, V. N. Kulkarni, J. Higgins, C. Lanci, J. R. Simpson, N. D. Browing, S. Das Sharma, H. D. Drew, R. l. Greene, and T. Venkatesan, Phys. Rev. Lett. **91**, 077205-1 (2003).
[15] J. M. D. Coey, A. P. Douvalis, C. B. Fitzgerald, and M. Venkatesan, Appl. Phys. Lett. **84**, 1332 (2004).
[16] C. B. Fitzgerald, M. Venkatesan, A. P. Douvalis, S. Huber, J. M. D. Coey, and T. Bakas, J. Appl. Phys. **95**, 7390 (2004).
[17] A. Punnoose, J. Hays, V. Gopal, and V. Shutthanandan, Appl. Phys. Lett. **85**, 1559 (2004).
[18] A. Punnoose, J. Hays, A. Thurber, M. H. Engelhard, R. K. Kukkadapu, C. Wang, V. Shutthanandan, and S. Thevuthasan, Phys. Rev. B **72**, 054402 (2005).
[19] J. Hays, A. Punnoose, R. Baldner, M. H. Engelhard, J. Peloquin, and K. M. Reddy, Phys. Rev. B **72**, 075203 (2005).
[20] MAUD, Materials Analysis Using Diffraction, by L. Lutterotti, 2002 Version: 1.84, http://www.ing.unitn.it/~maud/.
[21] W. H. Baur and A. A. Khan, Acta Crystallogr., Sect. B: Struct. Crystallogr. Cryst. Chem. **27**, 2133 (1971).
[22] S. R. Davis, A. V. Chadwick, and J. D. Wright, J. Phys. Chem. B **101**, 9901 (1997).
[23] C. Xu, J. Tamaki, N. Miura, and N. Yamazoe, Chem. Lett. **19**, 441 (1990).
[24] L. W. Finger and R. M. Hazen, J. Appl. Phys. **51**, 5362 (1980).
[25] D. C. Kundaliya, S. B. Ogale, S. E. Lofland, S. Dhar, C. J. Meting, S. R. Shinde, Z. Ma, B. Varughese, K. V. Ramanujachary, L. Salamanca-Riba, and T. Venkatesan, Nat. Mater. **3**, 709 (2004).
[26] C. Kilic and A. Zunger, Phys. Rev. Lett. **88**, 095501-1 (2002).
[27] C. Terrier, J. P. Chatelon, and J. A. Roger, Thin Solid Films **295**, 95 (1997).
[28] B. Grzeta, E. Tkalcec, C. Goebbert, M. Takeda, M. Takahashi, K. Nomura, and M. Jaksic, J. Phys. Chem. Solids **63**, 765 (2002).
[29] I. Saadeddin, H. S. Hilal, B. Pecquenard, J. Marcus, A. Mansouri, C. Labrugere, M. A. Subramanian, and G. Campet, Solid State Sci. **8**, 7 (2006).
[30] M. B. Stearns and Y. Cheng, J. Appl. Phys. **75**, 6894 (1994).
[31] K. Inaba, T. Hitosugi, Y. Hirose, Y. Furubayashi, G. Kinoda, Y. Yamamoto, T. W. Kim, H. Fujioka, T. Shimada, and T. Hasegawa, Jpn. J. Appl. Phys., Part 2 **45**, L114 (2006).
[32] L. A. Errico, M. Renteria, and M. Weissmann, Phys. Rev. B **72**, 184425 (2005).
[33] P. Xiaoyan, J. Dongmei, L. Yan, and M. Xueming, J. Magn. Magn. Mater. **305**, 388 (2006).
[34] G. Y. Ahn, S.-I. Park, I.-B. Shim, and C. S. Kim, J. Magn. Magn. Mater. **282**, 166 (2004).
[35] D. H. Kim, J. S. Yang, K. W. Lee, S. D. Bu, and T. W. Noh, S.-J. Oh, Y.-W. Kim, J.-S. Chung, H. Tanaka, H. Y. Lee, and T. Kawai, Appl. Phys. Lett. **81**, 2421 (2002).
[36] Y. J. Kim, S. Thevuthasan, T. Droubay, A. S. Lea, C. M. Wang, V. Shutthanandan, S. A. Chambers, R. P. Sears, B. Taylor, and B. Sinkovic, Appl. Phys. Lett. **84**, 3531 (2004).
[37] F. J. Berry, S. Skinner, and M. F. Thomas, J. Phys.: Condens. Matter **10**, 215 (1998).
[38] R. Monnier and B. Delley, Phys. Rev. Lett. **87**, 157204-1 (2001).
[39] G. Bouzerar and T. Ziman, Phys. Rev. Lett. **96**, 207602 (2006).
[40] A. M. Stoneham, *Theory of Defects in Solids* (Clarendon Press, Oxford, 1975), Chaps. 14–16.
[41] C. B. Fitzgerald, M. Venkatesan, L. S. Dorneles, R. Gunning, P. Stamenov, J. M. D. Coey, P. A. Stampe, R. J. Kennedy, E. C. Moreira, and U. S. Sias, Phys. Rev. B **74**, 115307 (2006).
[42] R. Janisch, and N. Spaldin, Phys. Rev. B **73**, 035201 (2006).
[43] L. Bergqvist, O. Eriksson, J. Kudrnovsky, V. Drchal, P. Korzhavyi, and I. Turek, Phys. Rev. Lett. **93**, 137202-1 (2004).
[44] A. H. Morrish, *Canted Antiferromagnetism: Haematite* (World Scientific, Singapore, 1994), Chap. 12.